Self-Seeded Growth of Germanium Nanowires: Coalescence and Ostwald Ripening

ARTICLE *in* CHEMISTRY OF MATERIALS · DECEMBER 2012

Impact Factor: 8.35 · DOI: 10.1021/cm3032863

8 AUTHORS, INCLUDING:

Johann Hlina
Graz University of Technology
12 PUBLICATIONS **68** CITATIONS
SEE PROFILE

Christoph Marschner
Graz University of Technology
143 PUBLICATIONS **1,620** CITATIONS
SEE PROFILE

Colm O'Dwyer
University College Cork
166 PUBLICATIONS **1,493** CITATIONS
SEE PROFILE

Nikolay Petkov
Tyndall National Institute
104 PUBLICATIONS **1,292** CITATIONS
SEE PROFILE

CHEMISTRY OF MATERIALS

Article

pubs.acs.org/cm

Self-Seeded Growth of Germanium Nanowires: Coalescence and Ostwald Ripening

Olan Lotty,[†,‡] Richard Hobbs,[†,‡] Colm O'Regan,[†,‡] Johann Hlina,[§] Christoph Marschner,[§] Colm O'Dwyer,[†] Nikolay Petkov,*[,†,‡] and Justin D. Holmes[†,‡]

[†]Materials Chemistry and Analysis Group and Applied Nanoscience Group, Department of Chemistry, University College Cork, Ireland and the Tyndall National Institute, University College Cork, Cork, Ireland

[‡]Centre for Research on Adaptive Nanostructures and Nanodevices (CRANN), Trinity College Dublin, Dublin 2, Ireland

[§]Institut für Anorganische Chemie der Technischen Universität Graz, Stremayrgasse 16, A-8010 Graz, Austria

Supporting Information

ABSTRACT: We report the controlled self-seeded growth of highly crystalline Ge nanowires, in the absence of conventional metal seed catalysts, using a variety of oligosilylgermane precursors and mixtures of germane and silane compounds (Ge:Si ratios between 1:4 and 1:1). The nanowires produced were encased in an amorphous shell of material derived from the precursors, which acted to isolate the Ge seed particles from which the nanowires were nucleated. The mode diameter and size distribution of the nanowires were found to increase as the growth temperature and Ge content in the precursors increased. Specifically, a model was developed to describe the main stages of self-seeded Ge nanowire growth (nucleation, coalescence, and Ostwald ripening) from the oligosilylgermane precursors and, in conjunction with TEM analysis, a mechanism of growth was proposed.

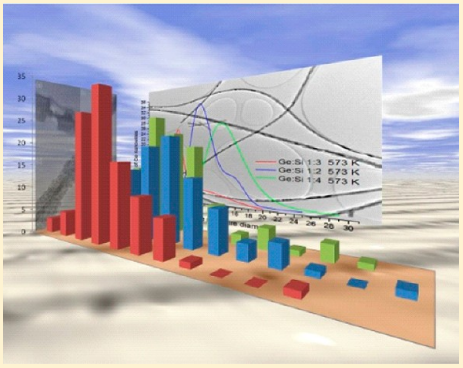

KEYWORDS: *germanium, nanowires, self-seeded, coalescence, Ostwald ripening*

INTRODUCTION

Germanium nanowires have attracted considerable interest as a channel material for field-effect transistors (FETs) because of their lower resistivity and high hole carrier mobility, compared to silicon nanowires.[1,2] Recently, Ge nanowires have also been utilized for lithium battery anode materials. Li^+ diffusion in Ge is 400 times higher than in Si,[3,4] while also possessing higher electrical conductivity (1×10^4), leading to the potential utilization of Ge in future high-rate Li-ion batteries. Furthermore, studies have shown that coating Ge nanowire electrodes with amorphous materials increases their reversible charge capacities.[5] The synthesis of Ge whiskers, via a vapor−liquid−solid (VLS) growth mechanism, was first reported by Bootsma et al.[6] in 1971 and the synthesis of Ge nanowires, using a solvothermal approach, was subsequently reported by Heath and co-workers in 1993.[7] Many methods have since been developed for generating Ge nanowires, which can be found in a number of comprehensive review articles.[8,9] A solution-based seedless approach has previously been reported by Chockla et al.;[10] however, their approach was based upon the decomposition of diphenylgermane (DPG) in high-boiling-point solvents. The Ge nanowire synthesis method progressed in this study is the lesser- reported self-seeded (or seedless) supercritical fluid (SCF) phase approach.[11] This self-seeded method does not rely on the growth of nanowires by a (noble) metal catalyst, but solely relies upon the decomposition of a metalorganic precursor to form a one-dimensional (1D) structure. While excellent levels of control over aspect ratios and scalability of semiconductor nanowires have been demonstrated using metal seeds, these catalysts can often contaminate, or uncontrollably dope, the growing nanowires.[12] For example, Korgel et al.,[13] reported that at a eutectic temperature of 363 °C Ge atoms dissolve in Au nanocrystals to form a liquid AuGe eutectic alloy. This eutectic, while crucial to the growth of the nanowires via a supercritical−fluid−liquid−solid mechanism, can also provide a pathway for the diffusion of metal atoms from the seed into the semiconductor nanowire material. Solid phase seeding mechanisms for growing Ge nanowires, such as those reported using Ni catalyst seeds, were at first thought to limit this diffusion, but recent electrical results indicate that inadvertent doping still occurs.[14]

Here we report the growth of Ge nanowires in the absence of conventional metal seeds using various mixtures of Ge and Si-containing precursors. Analysis of the diameter distributions of the nanowires revealed several trends in growth behavior, which can be directly linked to the precursor and temperature employed. We further propose that by analyzing the statistical diameter distributions of the nanowires formed, in addition to extensive morphological characterization by electron microscopy, the mechanism of nanowire growth can be inferred.

Received: October 11, 2012
Revised: December 19, 2012
Published: December 20, 2012

The coarsening of nanoparticles into nanowires via the self-seeded approach described in this article can occur through two fundamentally different mechanisms: (i) nanoparticles can move over a substrate, or within a matrix, to take part in binary collisions accompanied by liquidlike coalescence of the particles and (ii) the growth of nanowires can occur by the interparticle transport of single atoms from smaller nanoparticles to larger nanoparticles known as Ostwald ripening.[15] Nanowire growth (length) and broadening (diameter) originates from the supersaturated phase, which is still present in the system after the nucleation stage, and from concentration gradients around nanowires of different sizes.[16] The three main stages of growth (nucleation, coalescence and Ostwald ripening) are not sharply distinct, but in fact overlap during the evolution from a supersaturated phase to a ripened nanowire in the condensed phase.[17] We have combined a log-normal model for coalescence with a Gaussian model for Ostwald ripening to create an equation that accounts for this overlap. The nanowires in this article were synthesized with a variety of metalorganic precursors, which were deliberately tuned to alter the Ge:Si ratio; the ratios investigated were 1:4, 1:3, 1:2, and 1:1. The Ge nanowires produced had uniform core diameters and were coated with a nonuniform shell consisting of Si, Ge, O, and C. This amorphous coating was a byproduct of the precursor decomposition and plays an important role in the nanowire growth process.

EXPERIMENTAL SECTION

The oligosilylgermane precursors 1,2-bis[tris(trimethylsilyl)germyl]-tetramethyldisilane (Ge:Si 1:4), hexakis(trimethylsilyl)digermane (Ge:Si 1:3) and bis[tris(trimethylsilyl)germyl] dimethylgermane (Ge:Si 1:2) were synthesized following the procedures previously reported by Marschner et al.[18] For a 1:1 reaction mixture of Ge:Si, equal amounts of diphenylsilane (5 mM) and diphenylgermane (5 mM) were mixed together. The self-seeded growth of Ge nanowires was performed in supercritical toluene, as previously reported.[11] In a typical experiment, a 5 mL stainless steel reaction cell (HIP, USA) was loaded with 1 mL of anhydrous toluene and sealed inside a nitrogen filled glovebox. The reaction cell was then transferred to a tube furnace where it was heated to the desired reaction temperature and allowed to equilibrate for a period of 2 h. A Ge:Si precursor solution (10 mM), with a Ge:Si ratio of 1:4, 1:3, 1:2, or 1:1, was prepared in anhydrous toluene (10 mL) in a N_2 glovebox and loaded into a 20 mL stainless steel precursor reservoir (HIP, USA). This reservoir was then removed from the glovebox and connected to the reaction cell by 1/16″ stainless steel tubing and valves. A back pressure of 17.2 MPa was applied to the precursor reservoir; this solution was injected at the chosen synthesis temperature using a CO_2 pump (ISCO systems). The volume of the precursor solution injected into the cell was dependent on the pressure difference between the reaction cell and that of the precursor reservoir. Typically, 2.5 mL of precursor solution was injected into the reaction cell, and the holding time adjusted according to the temperature employed for a high yield of Ge nanowires.[11] The cell was opened at room temperature, and the initial solvent was collected and combined with an acetone solution used to collect the nanowire material attached to the side walls of the reactor. The typical yield for a reaction using the Ge:Si 1:3 precursor was between 50 and 100 mg and the other precursors yielded less than this. Energy-dispersive X-ray (EDX) analysis was performed using an Oxford Instruments INCA system fitted to a TEM. Powder X-ray Diffraction (PXRD) analysis was performed on a Phillips Xpert PW3719 diffractometer using Cu KR radiation (40 kV and 35 mA) over the range $10 < 2\theta < 70$. SEM imaging was carried out on a FEI Helios Nanolab dual-beam SEM/FIB suite operating at 5−10 kV. High resolution transmission electron microscopy (HRTEM) images were collected using a JEOL 2100 HRTEM instrument operating at an acceleration voltage of 200 kV. In-situ TEM heating stage experiments were performed using a Gatan 628 Single Tilt Heating Holder. In all cases, samples were prepared for analysis by sonicating the material in acetone before TEM sample preparation. Statistical analysis and modeling of the measured core diameter distributions of the nanowires was performed using Origin Pro v.8.5.1. and over 100 measurements were used for every nanowire diameter distribution (see the Supporting Information, Figures S3−S5).

MODELING NANOWIRE GROWTH

Links between the shape of diameter distributions of nanoparticles, nanoclusters, and microparticles and their methods of growth (coalescence or Ostwald ripening) were established as early as 1976.[15] Accordingly, a log-normal shape seen in the size distribution curve of nanoparticles implies that the primary mechanism for growth can be inferred as coalescence. In this article, we extend this relationship from nanoparticles, nanoclusters, and microparticles to nanowires. We believe that this scaling argument from nanoparticles to nanowires is reasonable when considering the diameters of the crystalline cores of the nanowires formed, not their lengths. The diameters of the nanowires in this study are of a similar (or even smaller) scale to previous nanoparticle and microparticle studies that consider the link between the shape of the particle size distributions and the coalescence and Ostwald ripening processes.[15,19,20] Ostwald ripening is often modeled with a function based upon the works of Lifshitz, Slyozof and Wagner.[21,22] Their combined methods have resulted in a model (LSW model), which is recognizable by its skewed distribution with a tail on the small diameter side of the diameter distributions. The LSW model also predicts that no particle greater than 1.5 times that of the mean particle diameter (in our case mean nanowire diameter) can exist. In reality, the particle size distributions are often skewed with a tail toward larger diameter sizes and particles greater than 1.5 times the average particle size often exist. The reason this upper limit exists is because LSW theory assumes that the system is infinitely dilute, which implies the absence of interparticle interactions.[23] When the stochastic process of interparticle interaction is taken into consideration, the LSW model must be altered and the artificial requirement that the particle size distribution, and all its derivatives, should go to zero above some finite value of particle size is removed.[16] To address these experimentally observed shortfalls with the LSW model, many groups have used a basic Gaussian function to model Ostwald ripening behavior and have reported much better fits to experimentally obtained particle size distributions.[16,20,24,25] A similar Gaussian function was incorporated into a model used by Conti et al.[26] who combined both coalescence and Ostwald ripening in a single model. Consequently, basic Gaussian and log-normal functions were combined to account for the coalescence of Ge particles into nanowires in this study, as shown in eq 1. Formation of the combined log-normal and Gaussian function in eq 1 is shown in the Supporting Information, Figure S2, along with deconvoluted data highlighting the individual contribution of both functions.

dx.doi.org/10.1021/cm3032863 | Chem. Mater. 2013, 25, 215−222

$$y = y_0 + \frac{A_c}{\sqrt{2\pi}}\exp\left(\frac{-\ln\left(\frac{x}{x_c}\right)^2}{2\sigma^2}\right) + \frac{A_r}{\sigma_1\sqrt{\frac{\pi}{2}}}\exp\left(\frac{-2(x - x_{cg})^2}{w_1^2}\right) \quad (1)$$

where A_c is the area under a log-normal curve, y_o is the baseline offset, x_c is the peak center of the log-normal contribution, σ is the standard deviation of the log-normal contribution, A_r is the area under a Gaussian curve, σ_1 is the width of a Gaussian curve (= fwhm/ln 4) and x_{cg} is the peak center of a Gaussian curve.

RESULTS AND DISCUSSION

Four different Ge:Si precursor solutions (Ge:Si 1:4, Ge:Si 1:3, Ge:Si 1:2, and Ge:Si 1:1), at four different reaction temperatures (573, 673, 723, and 773 K) were used to grow Ge nanowires via the SCF self-seeded approach. The corresponding diameter distributions for each sample were fitted using the combined log-normal/Gaussian function shown in eq 1. Table 1 below provides a summary of the log-normal peak center, x_c, and the Gaussian peak center, x_{cg}, fits, as determined by eq 1, for each of the Ge nanowire samples produced. Independent of the precursor used, the log-normal peak center was seen to increase with increasing growth temperature. The log-normal peak center also increased as the Ge:Si ratio changed from 1:3 to 1:1. Both of these trends highlight that larger diameter nanowires were achieved at high Ge concentrations and high growth temperatures; illustrating the temperature-dependence of the diffusion-limited growth process.

Table 1. Table Illustrating Trends in Log-Normal Peak Centers, x_c, (coalescence) and Gaussian Peak Centers, x_{cg}, (Ostwald ripening) for Synthesized Ge Nanowires As a Function of the Ge:Si Precursor Ratio and Reaction Temperature

		Ge:Si		
temp (K)		1:3	1:2	1:1
773	x_c	11.2 nm	---	17.4 nm
	x_{cg}	12.6 nm	21.8 nm	25.0 nm
723	x_c	7.6 nm	16.3 nm	21.4 nm
	x_{cg}	---	22.9 nm	---
673	x_c	7.2 nm	11.3 nm	13.3 nm
	x_{cg}	---	17.4 nm	---
573	x_c	6.2 nm	10.6 nm	14.4 nm
	x_{cg}	---	16.0 nm	---

Figure 1 shows the measured diameter distributions of self-seeded Ge nanowires formed using the Ge:Si 1:3 precursor as a function of temperature. A log-normal function fitted the diameter distribution of the nanowires grown at 573 K very well ($R^2 > 0.9$), with a primary peak centered at a diameter of 6 nm. Using the same precursor, experiments at 673 and 723 K yielded distributions with slightly larger primary peaks (7 and 8 nm, respectively) but still displayed a similar log-normal compliance. The small shoulder fitted on the large diameter side of the nanowire distribution (grown at 773 K) in Figure 1

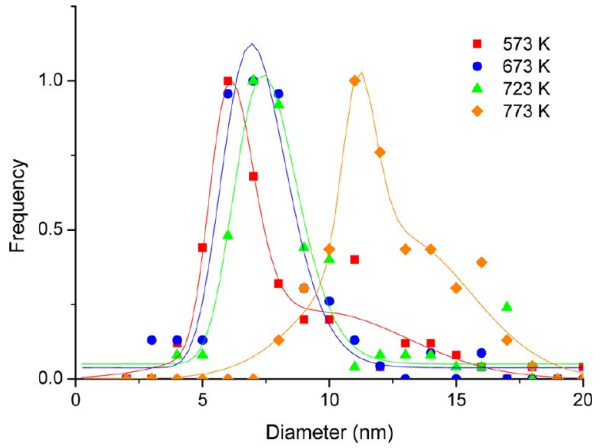

Figure 1. Diameter distributions of Ge nanowires grown from the Ge:Si 1:3 precursor at a reaction temperature of 573, 673, 723, and 773 K. A shift in the primary peak is observed as the growth temperature increases. The distributions of nanowire diameters were determined from TEM measurements of 100+ nanowires for each data set and fitted using a combined log-normal-Gaussian profile as detailed in eq 1.

may be attributed to the onset of Ostwald ripening behavior. This diameter distribution, fitted with a log-normal function on its own, yielded an R^2 value of 0.85. Using the combined log-normal/Gaussian function in eq 1 to account for the Ostwald ripening, an R^2 of 0.95 was achieved.

Although no length studies were performed on the nanowires produced, the vast majority of them examined by TEM exceeded 2 μm in length (Supporting Information, Figure S3–S5). More than 70% of the nanowires synthesized were orientated along the ⟨110⟩ direction, with the minority oriented along the ⟨111⟩ direction, which is consistent with previous reports.[11,27] Without exception, the mode seen in the diameter distributions of the Ge nanowires synthesized from the precursors increased with rising temperature and this is reflected in the log-normal peak centers summarized in Table 1. The driving force for any type of nucleation is an overall reduction of the Gibbs energy. A supersaturated solution will have an associated high chemical potential and the introduction of a solid phase through nucleation acts to lower this potential.[28,29] In the case of the mixed Ge:Si precursors, the supersaturation is the local Ge supersaturation within the Si-based matrix. The first stage in the growth of the Ge nanowires is the decomposition of the Ge:Si precursors to liberate the Ge atoms. From the relative bond dissociation energies, the Ge–Ge bond (263.6 kJ mol^{-1}) will be broken first, followed by the Ge–Si bonds (297 kJ mol^{-1}), followed by the Si–C bonds (451.5 kJ mol^{-1}), followed by the C–Ge bonds (455.7 kJ mol^{-1}). The liberation of Si atoms from the Ge precursor requires more energy than the liberation of Ge atoms and hence no Si or alloyed Si–Ge nanowires were observed in this study by either PXRD (see Figure S6 in the Supporting Information) or HRTEM. Liberated Ge atoms subsequently nucleate within the amorphous $SiO_xC_yH_z$ matrix, derived from the remainder of the precursor. This amorphous matrix is the shell material that surrounds the majority of the nanowires synthesized (see the Supporting Information, Figure S1). Following decomposition of the precursor, Ge nuclei are formed by microphase demixing followed by heterogeneous nucleation of Ge from the amorphous germanium-rich $Si_xO_yCH_z$ material. The amorphous material can act as a

dx.doi.org/10.1021/cm3032863 | Chem. Mater. 2013, 25, 215–222

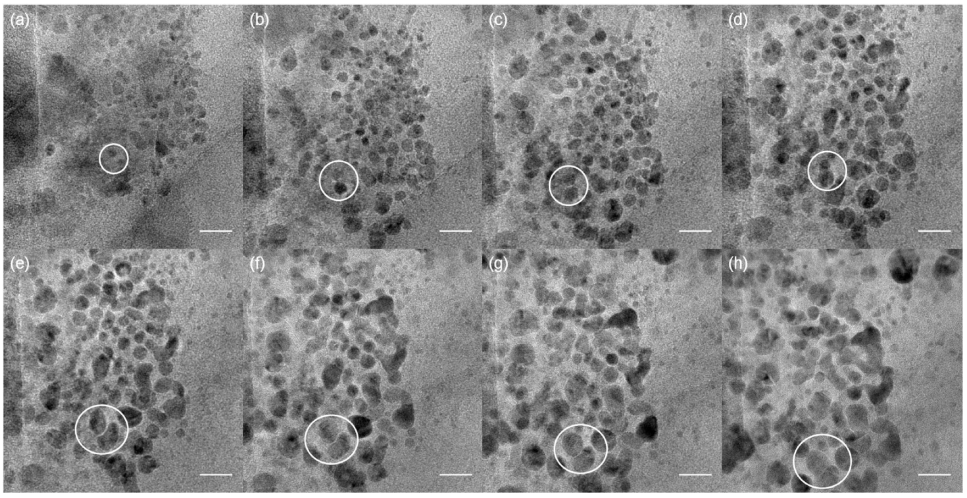

Figure 2. TEM sequence showing the nucleation, diameter broadening and coalescence of Ge nanoparticles from a Ge:Si (1:2) precursor under an electron beam (200 kV). The growth of one such particle is highlighted throughout the sequence by a white circle (scale bars = 20 nm).

support with nucleation sites of low activation energy barriers to seed the nucleation of the Ge nanoparticles. By nucleating at such sites, the Ge atoms contribute toward minimizing the total interfacial free energy of the system.[30] This theory is supported by the observation that no Ge nanowires form when using just diphenylgermane (DPG) as a precursor, suggesting that the $Si_xO_yCH_z$ component is needed in the self-seeded growth mechanism to provide the amorphous support for nucleation. The nuclei at this stage of growth are subject to a critical diameter depending on the precursor used and the growth temperature employed. As per nucleation theory, a critical radius exists for the nucleation of a particle. This critical radius is dependent on both concentration and temperature.[23] Nuclei below this dimension are unstable and retreat back into the amorphous $Si_xO_yCH_z$ material from which they were nucleated. It is possible that undecomposed precursor molecules or fragments of decomposed precursor molecules could be acting as surfactants which aid with this dissolution process. Nuclei that satisfy this dimensional requirement are stable and are able to grow and then coalesce together within the $Si_xO_yCH_z$ matrix to form Ge particles which in turn, coalesce or fuse to form elongated structures. Due to the melting point depression of nanoscale materials, these Ge nanoparticles may exist as liquid droplets, which solidify upon the creation of larger structures.[31] The liquid nature of these nanoparticles would explain their high mobility within the amorphous matrix.

Figure 2 shows a sequence of TEM images taken at 1 min intervals of some Ge:Si (1:2) precursor that was not fully decomposed from a reaction at 573 K. A large number of Ge nuclei can be observed within the Si-based matrix. Significantly, continued exposure of the Ge nanoclusters in the sample to the electron beam (200 kV) results in Ge nanoparticle nucleation, as shown in images a and b in Figure 2. Although the particular nucleation shown in Figure 2 is e-beam induced, it nonetheless offers an insight into the possible thermally induced nucleation that occurs from this same precursor material in the closed, pressurized reaction cell. Broadening of the particle size can be seen to occur in the latter part of the sequence; one such example is highlighted throughout the sequence by the white circles in Figure 2a–h. In Figure 2a–d, the two highlighted small particles can be seen to grow in size before coalescing together (Figure 2d). This process is then repeated again with the now larger particle in images e to h in Figure 2.

The aggregation of partially formed nanowires is evidenced by a "pinch" in the nanowire diameters often imaged by TEM. We postulate that these pinches occur at the sites where partially formed nanowires fuse together. These "pinched" sites offer evidence that the growth mechanism of the nanowires could involve the attachment of one elongated structure to another. The theory of attachment-oriented growth has been used to explain the seedless growth of PbS nanowires, also of a cubic crystal structure, by Yong et al.[32] They attributed the growth of PbS nanowires to the spontaneous alignment and fusion of PbS nanoparticles to form elongated structures and tentatively suggested that the alignment is a dipole-driven oriented aggregation of nanoparticles caused by exposed high-energy surface facets of the PbS crystal. However, the temporary dipoles in such structures are due to the charge balance that exists between metallic and nonmetallic faces. A more likely explanation for the attachment orientated growth of Ge nanostructures is that offered by Halder et al.[33] in their study of gold nanowires. They propose that a smoothing process, occurring between two faceted nanoparticles, provides a symmetry breaking mechanism that allows wire growth or elongation through the formation of a neck. The concave nature of the neck creates a negative potential on the wire to which atoms or clusters of atoms can diffuse from areas of higher potential, such as nearby flat or convex surfaces. This flux of material from areas of high to low chemical potential is shown schematically in Figure 3. The "healing" of defects within a coalescing crystal was also shown in the work of Ingham et al.[34] They studied the evolution of grain boundaries within coalescing Au nanoparticles and the subsequent disappearance of these grains. They also reference the formation of a neck between coalescing particles. However, they maintain that the grains (crystal defects) of the now coalesced particle still exist after coalescence and continue to grow before the defect density gradually reduces over time with further annealing. The grain growth stage takes much longer than the particle aggregation stage. This mechanism is also possible within our system, although perpendicular twin boundaries or defects have not been observed in fully formed nanowires grown in our experiments. However, these attach-

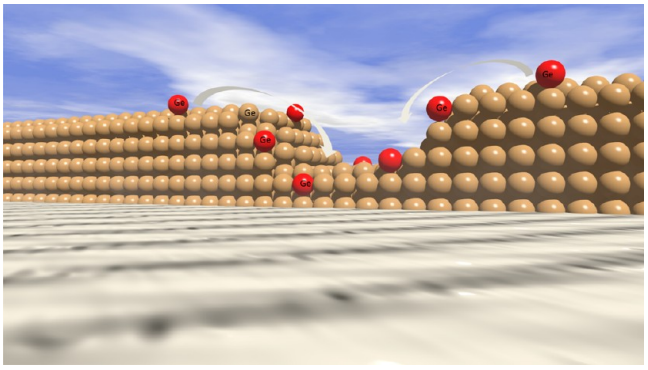

Figure 3. Schematic showing the diffusion of Ge atoms from flat or convex sites of high chemical potential to concave sites of low chemical potential.

ment-orientated growth theories do not ultimately explain why the Ge nanoparticles in the amorphous $Si_xO_yCH_z$ matrix, would attach in an anisotropic manner. One possibility is that the liquid nanoparticles coalesce to form an elongated structure, which subsequently crystallizes. This is similar to the growth mechanism proposed by Ge et al.[35] for their seedless growth of Ge nanowires, where nanowires with a cubic structure along the [110] direction were formed by the attachment of liquid Ge droplets to form cubic crystalline nanowires. In our system, the amorphous material that coats the nanowires, (Figure 4b, c and Figure S6 in the Supporting Information) potentially passivates the surfaces of these elongated Ge nanostructures at their surface, thus encouraging the attachment of more liquid nanoparticles to their ends. This would also explain why no

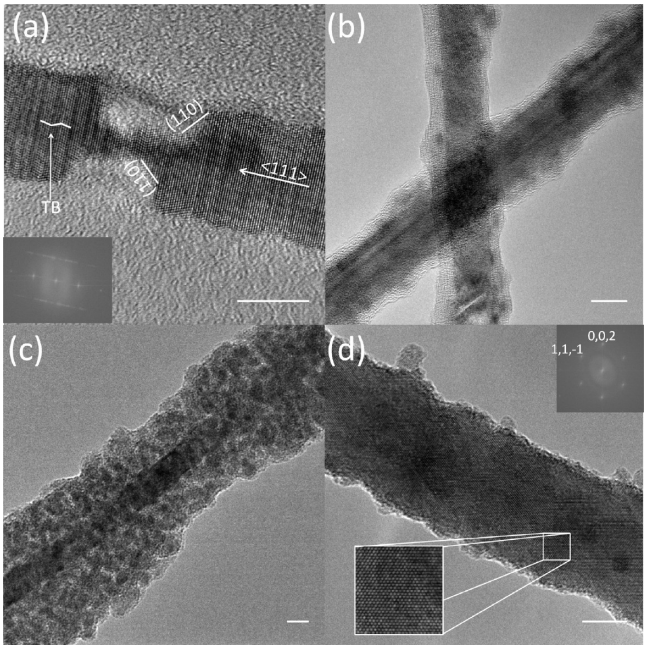

Figure 4. High-resolution TEM images of (a) a "pinch" in a Ge nanowire with growth direction, high energy surface facets, and twinning boundaries (TB) highlighted (insert: FFT displaying the twinning relationship), (b) Ge nanowires with amorphous shells, (c) Ge nanowire with an amorphous shell containing Ge nanoparticles, and (d) Ge nanowire without an amorphous shell. Inset in d shows the highly crystalline nature of the nanowires and the FFT illustrates the ⟨111⟩ growth direction (scale bars = 10 nm).

dendritic or branched Ge nanowire structures were seen in this study. The preferential attachment of the amorphous material to side facets, rather than the end facets of the Ge structure, could be analogous to a DFT study which found that the fraction of bound sites for amines on gold to {111} surfaces is much lower than those to {100} surfaces.[33,36]

The smoothing process of the above-described "pinch" sites was evidenced in both the gold nanowires synthesized by Halder et al.[33] and the Ge nanowires grown in this study, due to the formation of coherent twin boundaries as highlighted in Figure 4a. The twin formation is also highlighted by the FFT of the nanowire inset in Figure 4a, which clearly shows the twin relationship, i.e., where one set of planes remain continuous while the other set of {111} planes are related by a mirror symmetry across the boundary. FFT analysis of both sides of the neck in Figure 4a show that they are both orientated along the same growth direction. The coherent twin boundary, being a very low-energy interface for Ge (ca. ~30 mJ m^{-2}), gives rise to this possibility.[37] The pinch site is therefore eventually normalized with the rest of the nanowire diameter by Ge nuclei that continue to diffuse onto the surface due to the negative radius of curvature associated with a concave notch. Once this crystalline structure is formed, Ge nuclei continue to diffuse to the nanowire surface and small Ge particles can be seen to occupy the amorphous shell material that surrounds these wires (Figure 4c). In the final product, only very few Ge nanoparticles were seen to exist outside of the nanowire shells. The shell material on the nanowires was more evident at higher growth temperatures (723 and 773 K). Nanowires formed at lower growth temperatures (573 and 673 K) often exhibit wires with overall thinner, or nonexistant, shells, as shown in Figure 4d. Changing from the 3:1 precursor to the 1:1 precursor did not alter this trend and the thickness of the shell was not uniform for any reaction temperature (see Figure S6 in the Supporting Information). Often nanowires of the same diameter had shells of different mean thicknesses.

As the growth temperature was increased, there was an increase in the rate of diffusion of Ge within the $Si_xO_yCH_z$ matrix, leading to a broadening of the nanowire diameter through diffusion-limited Ostwald ripening,[38] as shown by the TEM images in Figure 5 of an in situ heating stage experiment. As the temperature is increased, the nanowire diameter is broadened from 14 nm at 303 K to almost 23 nm at 723 K. Although the diameter is not observed to increase uniformly along the length of the nanowire (due to the very different reaction environment in the TEM compared to the SCF experimental conditions), the data demonstrates the important role of the shell in the nanowire growth process.

The expansion of the mean nanowire diameter with increasing Ge:Si ratio could be indirectly related to the ease by which Ge atoms are liberated from each of the precursors. However, the 1:2 precursor requires more energy to liberate a Ge atom than the 1:3 precursor, but still produces nanowires with a larger mode diameter (see table 1). A more likely explanation for the trend would be the increased amount of Ge compared to silicon in the precursors and the dynamics of the coalescence and ripening processes of Ge in the $Si_xO_yCH_z$ matrix. Although the Ge atomic concentration in the precursors increases upon moving from Ge:Si 1:4 toward 1:1, the increase in the mode diameters observed are primarily due to the increasing Ge:Si ratio and not the total atomic concentration of Ge. To prove this hypothesis, we matched the Ge:Si 1:3 and 1:2 precursors in their atomic concentration of Ge (0.034 M)

dx.doi.org/10.1021/cm3032863 | Chem. Mater. 2013, 25, 215−222

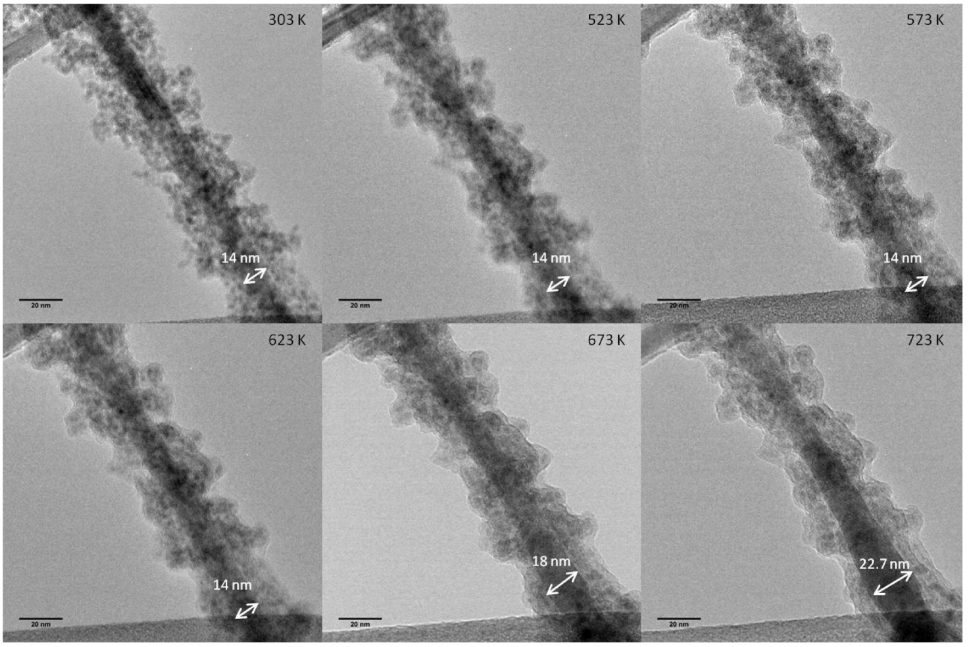

Figure 5. In situ TEM heating stage experiments showing the Ge nanowire diameter increasing with temperature. The diffusion of Ge particles from the shell to the crystalline core increases with temperature.

and nanowires were grown from both precursors at 573 K. The diameter distributions of both nanowire products were compared and the 1:2 precursor consistently yielded nanowires with a larger mode diameter than nanowires obtained from the 1:3 precursor. An increased Ge:Si ratio therefore leads to the growth of Ge nanowires with larger mode diameters. Diffusion-limited growth of nanowires is directly related to the solute concentration in a system, which in this study was controlled by the Ge:Si ratio, where the Si forms the amorphous $Si_xO_yCH_z$ medium through which the Ge must diffuse. Fick's first law of diffusion (eq 2), states that the flux of matter between areas of high and low concentration is directly proportional to the concentration gradient that exists between these two areas of Ge content.

$$J = -D\Delta c \tag{2}$$

where J = flux (mol m^{-2} s^{-1}), D is the diffusion coefficient (m^2 s^{-1}), and Δc is the concentration gradient. The coefficient of proportionality in this flux-concentration relationship, known as the diffusion coefficient, D, is also temperature-dependent and is a function of the mean free path and mean thermal speed. As the mean thermal speed increases with temperature, the diffusivity of the nucleating clusters also increases with temperature.[39] Consequently, longer, broader wires are formed at higher temperatures and at a higher Ge content.

The oligosilylgermane precursors decomposed to form matrices, composing of varying compositions of C, H, Si, Ge, and O, from which the Ge nanowires nucleated. As the Ge content in the Ge:Si (1:4) is comparatively small compared to Si, a reduced number of Ge nucleation events will occur compared to the other precursors investigated. The low Ge content effectively lowers the quantity of Ge atoms that can diffuse to a certain nucleus within the amorphous matrix, and no nanowire growth was observed over a reaction time of 24 h at 673 K. The observations from the Ge:Si (1:4) precursor suggests that a certain threshold concentration exists, below which insufficient nucleation occurs via diffusion. The observed threshold concentration is overcome by altering the Ge:Si ratio from 1:4 to 1:3, resulting in sufficient Ge nucleation events to generate small diameter (6 nm) Ge nanowires. As the Ge:Si ratio was increased further to 1:2 and 1:1, the mode diameter of the nanowires synthesized increased from 6 to 11 nm respectively, as is highlighted in figure 6 below. A comparison

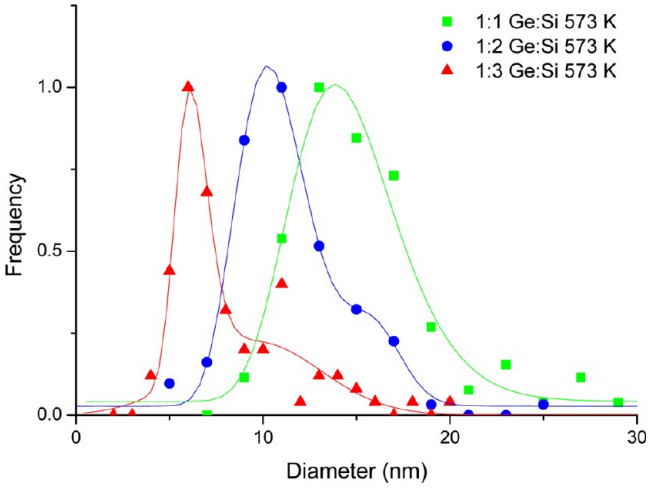

Figure 6. Fitting function of Ge nanowires formed at 573 K using the Ge:Si 1:3, Ge:Si 1:2, and Ge:Si 1:1 precursors, respectively, highlighting the mode diameter shift of the nanowires generated. The distributions were determined from TEM measurements of 100+ nanowires for each sample and fitted using the combined log-normal-Gaussian function given in eq 1.

of experiments performed at 573 K show the peak centers (or mode diameters) at 6, 11, and 14 nm for the Ge:Si 1:3, Ge:Si 1:2 and Ge:Si 1:1 precursors, respectively. Ostwald ripening becomes dominant when the Ge:Si ratio shifts from 1:3 toward 1:1. This increase in Ostwald ripening behavior is reflected in the diameter distributions, which are fitted with a Gaussian-like profile. At a Ge:Si ratio of 1:1, all of the Ge nanowires formed

dx.doi.org/10.1021/cm3032863 | Chem. Mater. 2013, 25, 215−222

undergo so much broadening that no evidence remains of the coalescence that preceded this Ostwald ripening and so the log-normal contribution of the fitting function is effectively reduced to zero.

As previously discussed, Ge nanowires synthesized at a low temperature, e.g., 573 K, and from precursors with a low Ge content, e.g., Ge:Si (1:3), tended to show a log-normal type diameter distribution indicative of coalescence. Experiments at higher temperatures, e.g., 773 K, and from precursors with a high Ge content, e.g., Ge:Si (1:1), displayed a more Gaussian nanowire diameter distribution, indicative of Ostwald ripening. Many experiments, however, showed nanowire diameter distributions that displayed evidence of both coalescence and Ostwald ripening and were modeled using an equal contribution from both the log-normal and Gaussian terms, such as the Ge:Si ratio of 1:2 at 723 K.

CONCLUSIONS

Ge nanowires have been successfully grown without the introduction of a foreign seed particle from various mixed Ge/Si precursors. A model has been proposed that accounts for nanoparticle coalescence at the beginning stage of nanowire growth and Ostwald ripening in the latter stages of growth. Analysis of the nanowire diameter distributions revealed several trends which can be directly related to the Ge:Si ratio of the precursor employed and the growth temperature. We have shown that the information yielded from analysis of diameter distributions can aid the understanding of growth mechanisms in nanowire growth experiments. This study also highlights the possibility of achieving Ge nanowire diameter control through the engineering of various Ge precursor molecules.

ASSOCIATED CONTENT

Supporting Information

Combined TEM/EDX data for nanowires grown. Detail of fitting function described in eq 1. Fitted diameter distributions for all growth experiments conducted in this study. Low resolution TEM images of nanowires grown. SEM images of nanowires grown. PXRD pattern of nanowires grown. This material is available free of charge via the Internet at http://pubs.acs.org.

AUTHOR INFORMATION

Corresponding Author

*Tel: +353 (0)21 4903608. Fax: +353 (0)21 4274097. E-mail: j.holmes@ucc.ie.

Author Contributions

The manuscript was written through contributions of all authors. All authors have given approval to the final version of the manuscript.

Notes

The authors declare no competing financial interest.

ACKNOWLEDGMENTS

The authors acknowledge financial support from the European Union 7th Framework Programme under the SiNAPS project (project ref: 257856), the Irish Research Council for Science, Engineering and Technology (IRCSET) for an EMBARK scholarship to C.O.R., and Science Foundation Ireland (SFI), project ref: 08/CE/I1432.

REFERENCES

(1) Wu, X. Y.; Kulkarni, J. S.; Collins, G.; Petkov, N.; Almecija, D.; Boland, J. J.; Erts, D.; Holmes, J. D. *Chem. Mater.* **2008**, *20* (19), 5954−5967.
(2) Hanrath, T.; Korgel, B. A. *J. Am. Chem. Soc.* **2004**, *126* (47), 15466−15472.
(3) Graetz, J.; Ahn, C. C.; Yazami, R.; Fultz, B. *J. Electrochem. Soc.* **2004**, *151* (5), A698−A702.
(4) Laforge, B.; Levan-Jodin, L.; Salot, R.; Billard, A. *J. Electrochem. Soc.* **2008**, *155* (2), A181−A188.
(5) Seo, M. H.; Park, M.; Lee, K. T.; Kim, K.; Kim, J.; Cho, J. *Energy Environ. Sci.* **2011**, *4* (2), 425−428.
(6) Bootsma, G. A.; Gassen, H. J. *J. Cryst. Growth* **1971**, *10* (3), 223−&.
(7) Heath, J. R.; LeGoues, F. K. *Chem. Phys. Lett.* **1993**, *208* (3−4), 263−268.
(8) Hobbs, R. G.; Petkov, N.; Holmes, J. D. *Chem. Mater.* **2012**, *24* (11), 1975−1991.
(9) Barth, S.; Hernandez-Ramirez, F.; Holmes, J. D.; Romano-Rodriguez, A. *Prog. Mater Sci.* **2010**, *55* (6), 563−627.
(10) Chockla, A. M.; Korgel, B. A. *J. Mater. Chem.* **2009**, *19* (7), 996−1001.
(11) Hobbs, R. G.; Barth, S.; Petkov, N.; Zirngast, M.; Marschner, C.; Morris, M. A.; Holmes, J. D. *J. Am. Chem. Soc.* **2010**, *132* (39), 13742−13749.
(12) Allen, J. E.; Hemesath, E. R.; Perea, D. E.; Lensch-Falk, J. L.; LiZ., Y.; Yin, F.; Gass, M. H.; Wang, P.; Bleloch, A. L.; Palmer, R. E.; Lauhon, L. J. *Nat Nano* **2008**, *3* (3), 168−173.
(13) Holmberg, V. C.; Collier, K. A.; Korgel, B. A. *Nano Lett.* **2011**, *11* (9), 3803−3808.
(14) Barth, S.; Koleśnik, M. M.; Donegan, K.; Krstić, V.; Holmes, J. D. *Chem. Mater.* **2011**, *23* (14), 3335−3340.
(15) Granqvist, C. G.; Buhrman, R. A. *J. Catal.* **1976**, *42* (3), 477−479.
(16) Senkov, O. N. *Scripta Mater.* **2008**, *59* (2), 171−174.
(17) Madras, G.; McCoy, B. J. *Chem. Eng. Sci.* **2002**, *57* (18), 3809−3818.
(18) Fischer, J.; Baumgartner, J.; Marschner, C. *Organometallics* **2005**, *24* (6), 1263−1268.
(19) Gregori, G.; Kleebe, H. J.; Readey, D. W.; Soraru, G. D. *J. Am. Ceram. Soc.* **2006**, *89* (5), 1699−1703.
(20) Senkov, O. N.; Shagiev, M. R.; Senkova, S. V.; Miracle, D. B. *Acta Mater.* **2008**, *56* (15), 3723−3738.
(21) Lifshitz, I. M.; Slyozov, V. V. *J. Phys. Chem. Solids* **1961**, *19* (1−2), 35−50.
(22) Wagner, C. *Z. Elektrochem* **1961**, *65* (7−8), 581−591.
(23) Finsy, R. *Langmuir* **2004**, *20* (7), 2975−2976.
(24) Ma, Y.; Ardell, A. J. *Acta Mater.* **2007**, *55* (13), 4419−4427.
(25) Ges, A. M.; Fornaro, O.; Palacio, H. A. *Mater. Sci. Eng. A-Struct. Mater. Prop. Microstruct. Process* **2007**, *458* (1−2), 96−100.
(26) Conti, M.; Meerson, B.; Peleg, A.; Sasorov, P. V. *Phys. Rev. E* **2002**, *65*, 4.
(27) Schmidt, V.; Senz, S.; Gosele, U. *Nano Lett.* **2005**, *5* (5), 931−935.
(28) Mullin, J. W., *Crystallization*; Elsevier Science: Amsterdam, 2001.
(29) Auer, S.; Frenkel, D. *Nature* **2001**, *413* (6857), 711−713.
(30) Zheng, F.; Chew, H. G.; Choi, W. K.; Zhang, J. X.; Seng, H. L. *J. Appl. Phys.* **2007**, *101* (11), 114310.
(31) Qi, W. H.; Wang, M. P. *Mater. Chem. Phys.* **2004**, *88* (2−3), 280−284.
(32) Yong, K. T.; Sahoo, Y.; Choudhury, K. R.; Swihart, M. T.; Minter, J. R.; Prasad, P. N. *Chem. Mater.* **2006**, *18* (25), 5965−5972.
(33) Halder, A.; Ravishankar, N. *Adv. Mater.* **2007**, *19* (14), 1854.
(34) Ingham, B.; Lim, T. H.; Dotzler, C. J.; Henning, A.; Toney, M. F.; Tilley, R. D. *Chem. Mater.* **2011**, *23* (14), 3312−3317.
(35) Ge, M.; Liu, J. F.; Wu, H.; Yao, C.; Zeng, Y.; Fu, Z. D.; Zhang, S. L.; Jiang, J. Z. *J. Phys. Chem. C* **2007**, *111* (30), 11157−11160.

(36) Pong, B. K.; Lee, J. Y.; Trout, B. L. *Langmuir* **2005**, *21* (25), 11599−11603.
(37) Davidson, F. M.; Lee, D. C.; Fanfair, D. D.; Korgel, B. A. *J. Phys. Chem. C* **2007**, *111* (7), 2929−2935.
(38) Chew, H. G.; Choi, W. K.; Foo, Y. L.; Zheng, F.; Chim, W. K.; Voon, Z. J.; Seow, K. C.; Fitzgerald, E. A.; Lai, D. M. Y. *Nanotechnology* **2006**, *17* (8), 1964−1968.
(39) Atkins, P. W., *Physical Chemistry*, 4th ed.; Freeman: New York, 1990.